Supporting Information

Multidentate 2-pyridyl-phosphine ligands – towards ligand tuning and chirality

Schirin Hanf,[a] Raúl García-Rodríguez,[a] Sascha Feldmann,[a] Andrew D. Bond,[a] Evamarie Hey-Hawkins*[,b] and Dominic S. Wright*[,a]

[a] Chemistry Department, University of Cambridge, Lensfield Road, CB2 1EW, Cambridge, UK.
[b] Institute of Inorganic Chemistry, Faculty of Chemistry and Mineralogy, Leipzig University, Johannisallee 29, 04103 Leipzig, Germany.

1. DFT calculations on [{$(Me_2N)P(2\text{-}py)_2$}$(LiCl)_3 \cdot 2THF]_2$ ([1$(LiCl)_3 \cdot 2THF]_2$) and $(Et_2N)_2P(2\text{-}py)$ (2)

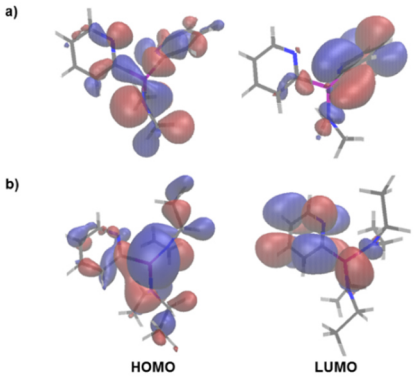

Figure S1. The HOMO (left) and LUMO (right) of **1** (a) without LiCl and **2** (b) at an isovalue of ± 0.02, B3LYP, 6.31g** level of theory.

2. Representative NMR spectra for selected compounds

a) NMR spectra of pyridyl-phosphines

NMR spectra of [{(Me$_2$N)P(2-py)$_2$}(LiCl)$_3$·2THF]$_2$ (1(LiCl)$_3$·2THF]$_2$)

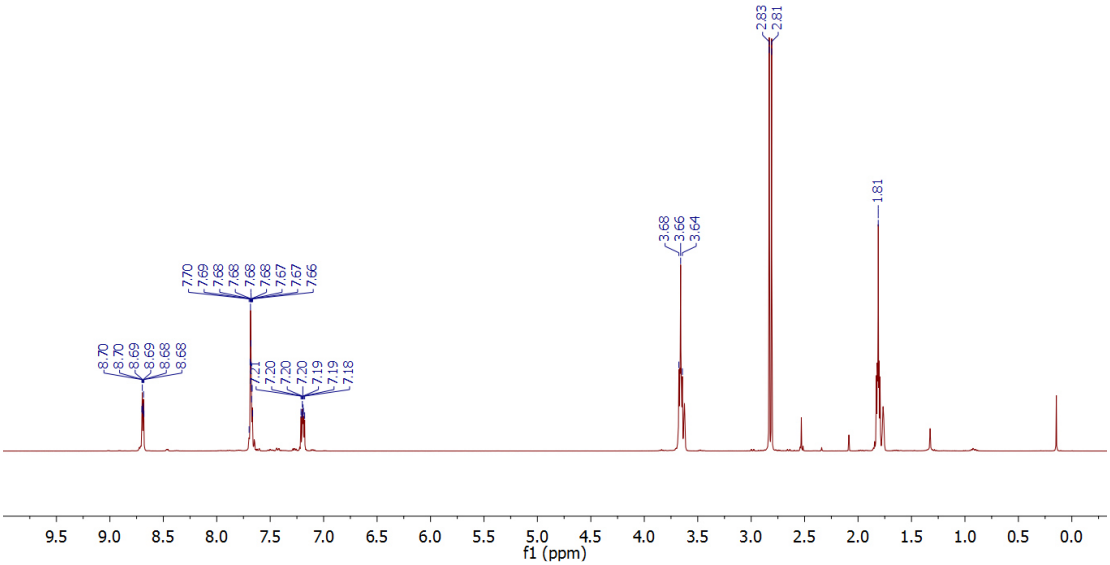

Figure S2. ^{1}H NMR (400.13 MHz, d$_8$-THF, 298 K) spectrum of [{(Me$_2$N)P(2-py)$_2$}(LiCl)$_3$·2THF]$_2$ (**1**(LiCl)$_3$·2THF]$_2$).

Note: The d$_8$-THF solvent residual signal partially overlaps with the signal of the coordinated THF molecules at 1.81 ppm and 3.66 ppm.

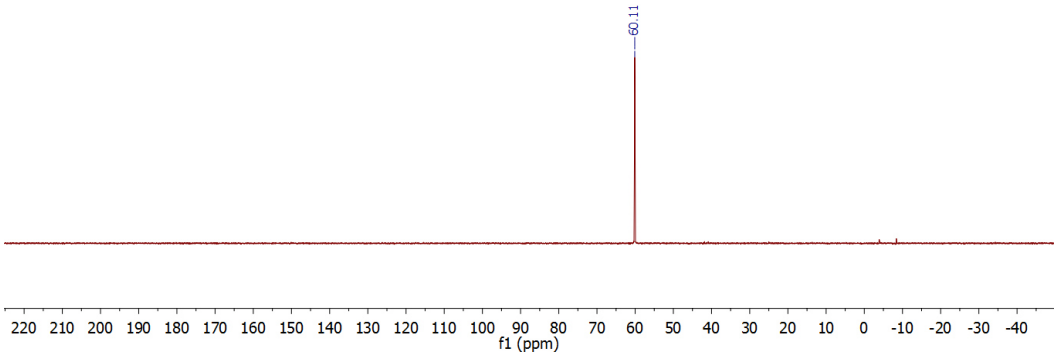

Figure S3. ^{31}P{^{1}H} NMR (161.98 MHz, d$_8$-THF, 298 K) spectrum of [{(Me$_2$N)P(2-py)$_2$}(LiCl)$_3$·2THF]$_2$ (**1**(LiCl)$_3$·2THF]$_2$).

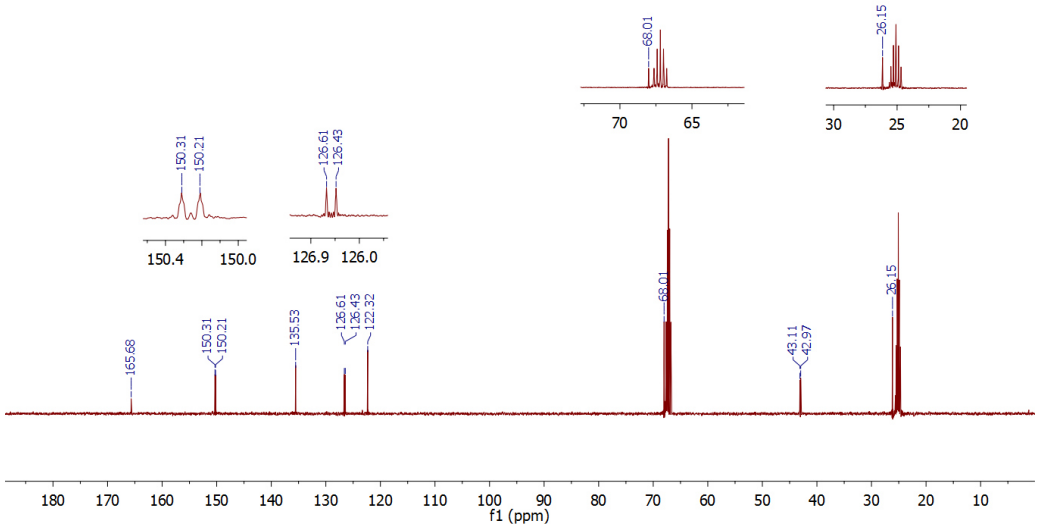

Figure S4. ^{13}C{^{1}H} NMR (100.61 MHz, d$_8$-THF, 298 K), spectrum of [{(Me$_2$N)P(2-py)$_2$}(LiCl)$_3$·2THF]$_2$ (**1**(LiCl)$_3$·2THF]$_2$).

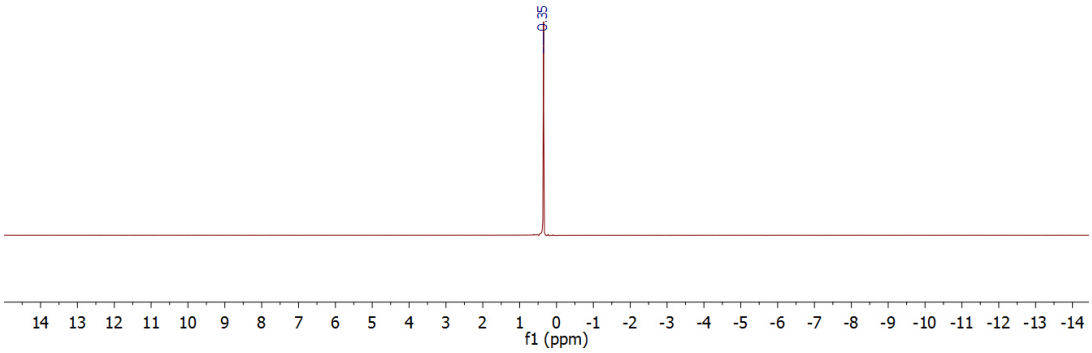

Figure S5. $^{7}Li\{^{1}H\}$ NMR (155.51 MHz, d_8-THF, 298 K) spectrum of $[\{(Me_2N)P(2\text{-}py)_2\}(LiCl)_3{\cdot}2THF]_2$ (**1**$(LiCl)_3{\cdot}2THF]_2$).

NMR spectra of $(Et_2N)_2P(2\text{-}py)$ (2)

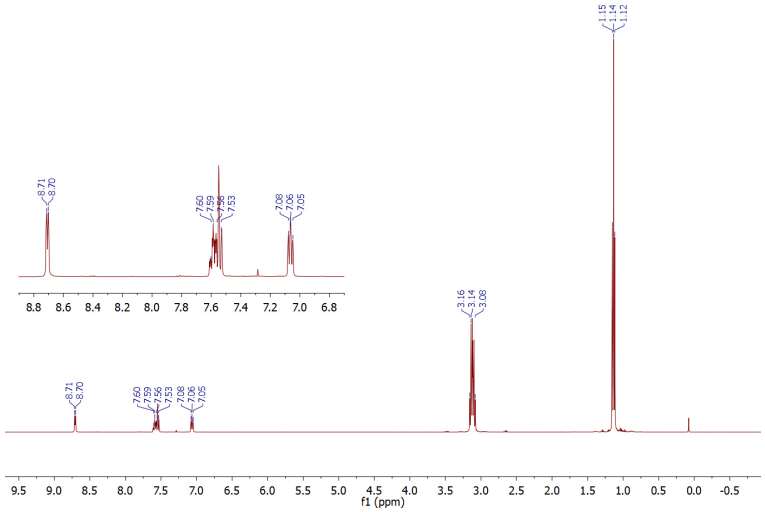

Figure S6. ^{1}H NMR (400.13 MHz, $CDCl_3$, 298 K) spectrum of $(Et_2N)_2P(2\text{-}py)$ (**2**).

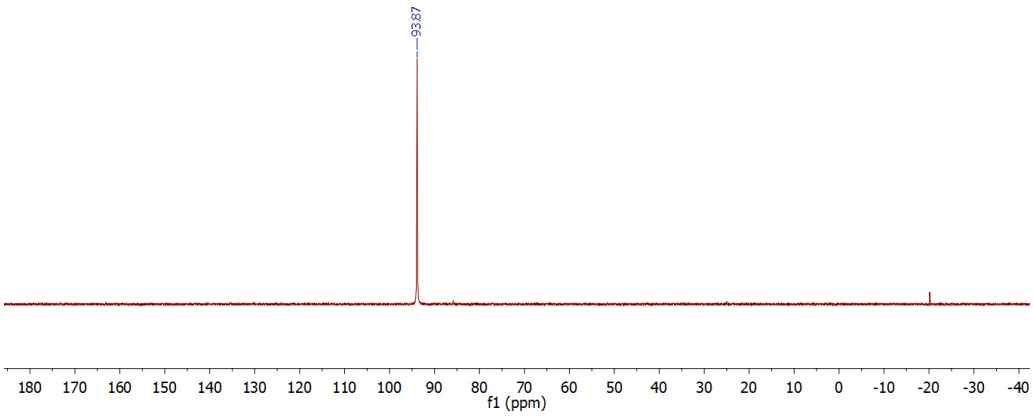

Figure S7. $^{31}P\{^{1}H\}$ NMR (161.98 MHz, $CDCl_3$, 298 K) spectrum of $(Et_2N)_2P(2\text{-}py)$ (**2**).

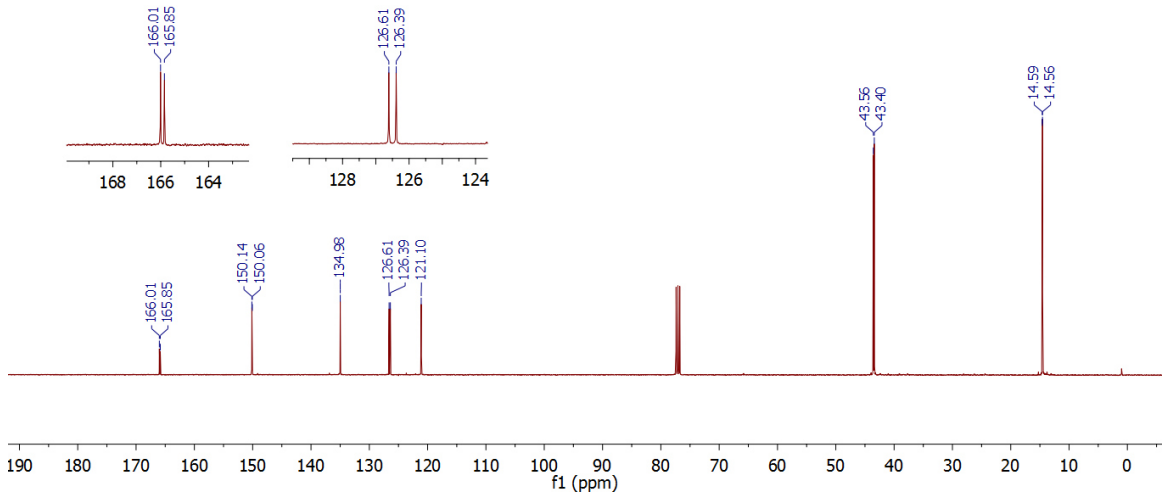

Figure S8. $^{13}C\{^{1}H\}$ NMR (100.63 MHz, $CDCl_3$, 298 K) spectrum of $(Et_2N)_2P(2\text{-py})$ (**2**).

NMR spectra of $(Et_2N)PhP(2\text{-py})$ (3)

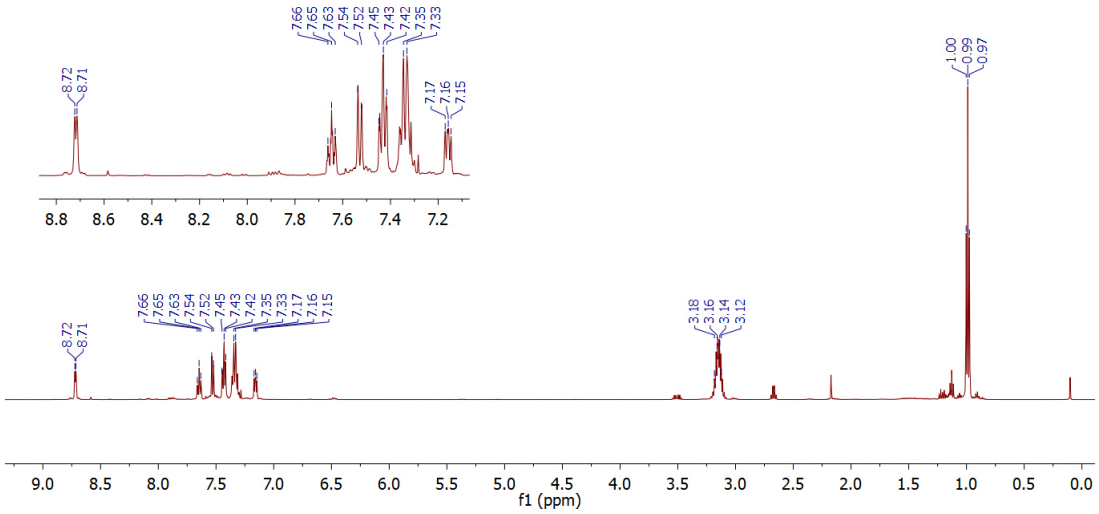

Figure S9 ^{1}H NMR (500.20 MHz, $CDCl_3$, 298 K) spectrum of $(Et_2N)PhP(2\text{-py})$ (**3**).

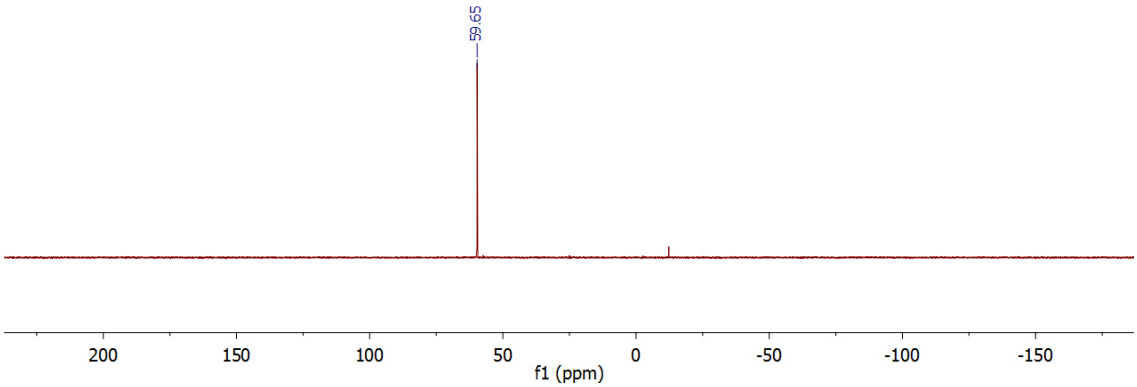

Figure S10. $^{31}P\{^{1}H\}$ NMR (161.98 MHz, $CDCl_3$, 298 K) spectrum of $(Et_2N)PhP(2\text{-py})$ (**3**).

Note: A small amount of an impurity at -12.3 ppm (4 %) was observed, since compound **3** readily oxidises or hydrolyses in the NMR tube after prolonged storage.

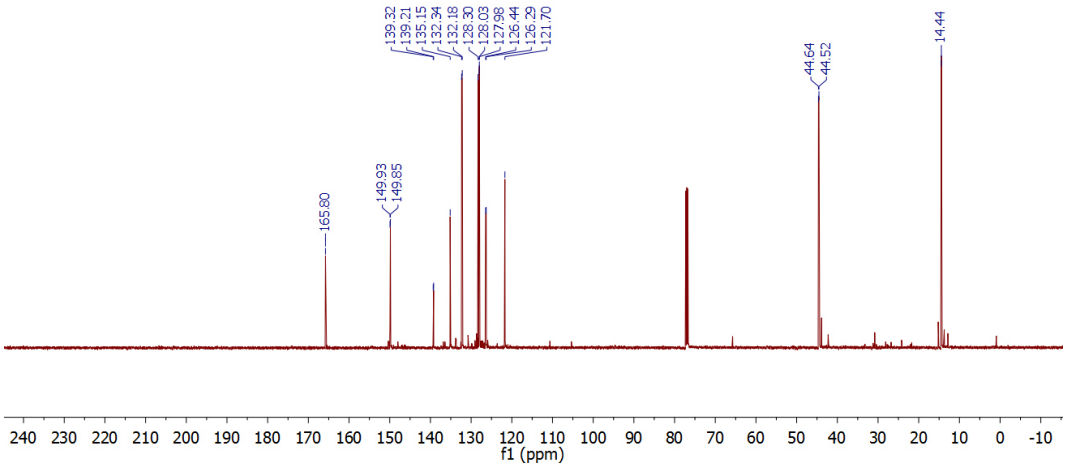

Figure S11. $^{13}C\{^{1}H\}$ NMR (125.78 MHz, $CDCl_3$, 298 K) spectrum of $(Et_2N)PhP(2\text{-py})$ (**3**).

NMR spectra of [{(MeO)P(2-py)$_2$}LiCl]$_2$ ([**4**·LiCl]$_2$)

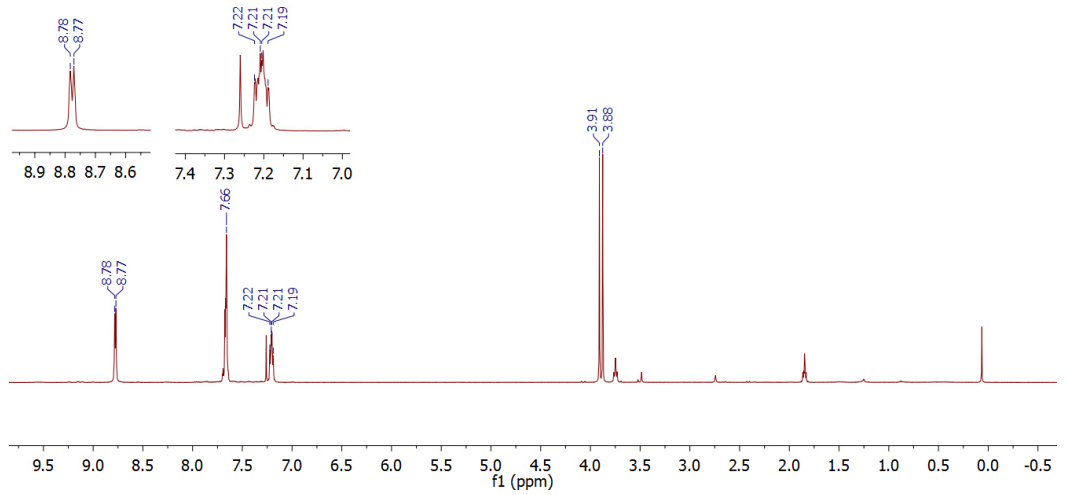

Figure S12. ^{1}H NMR (400.13 MHz, $CDCl_3$, 298 K) spectrum of [{(MeO)P(2-py)$_2$}LiCl]$_2$ ([**4**·LiCl]).

Note: THF is present in the spectrum (multiplets at 1.85 ppm and 3.75 ppm).

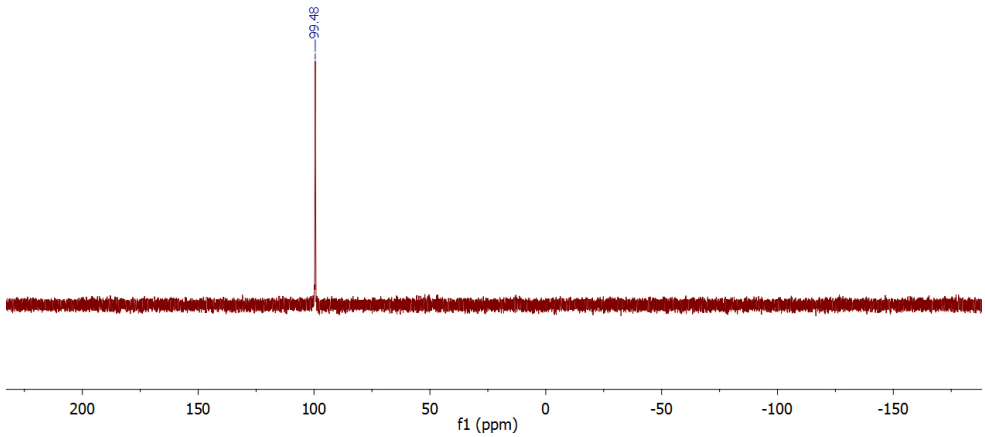

Figure S13. $^{31}P\{^{1}H\}$ NMR (161.98 MHz, $CDCl_3$, 298 K) spectrum of [{(MeO)P(2-py)$_2$}LiCl]$_2$ ([**4**·LiCl]).

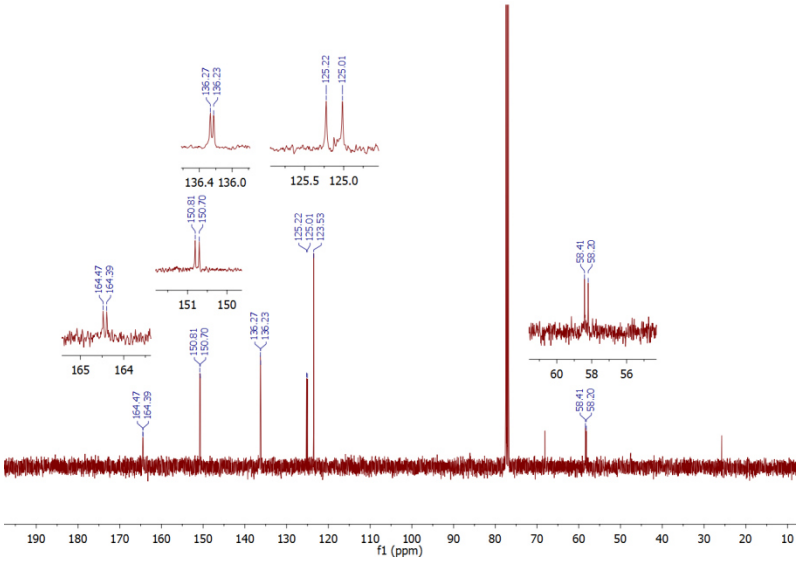

Figure S14. $^{13}C\{^{1}H\}$ NMR (100.61 MHz, $CDCl_3$, 298 K) spectrum of [{(MeO)P(2-py)$_2$}LiCl]$_2$ ([**4**·LiCl]).

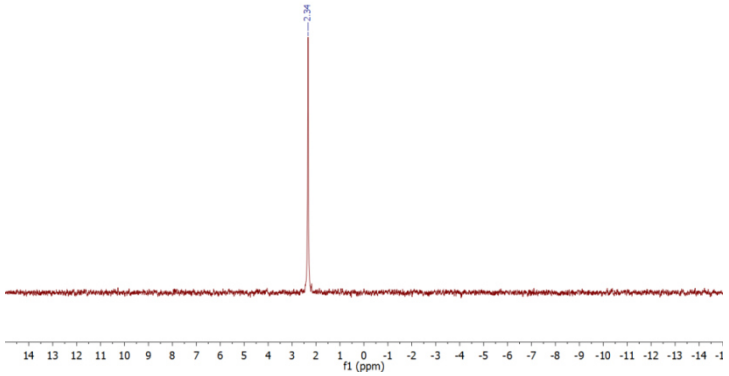

Figure S15. $^{7}Li\{^{1}H\}$ NMR (155.51 MHz, $CDCl_3$, 298 K) spectrum of [{(MeO)P(2-py)$_2$}LiCl]$_2$ ([**4**·LiCl]).

NMR spectra of [{(2-BuO)P(2-py)$_2$}LiCl]$_2$ ([**5**·LiCl]$_2$)

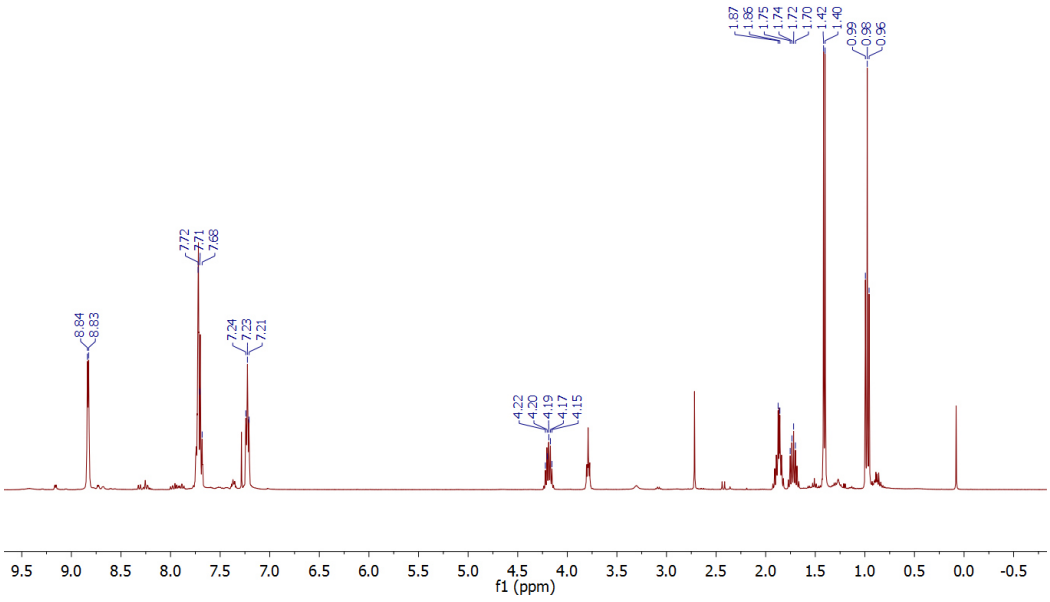

Figure S16 ^{1}H NMR (400.13 MHz, $CDCl_3$, 298 K) spectrum of [{(2-BuO)P(2-py)$_2$}LiCl]$_2$ ([**5**·LiCl]$_2$).

Note: The multiplets at 1.85 ppm (overlapping with the signal of the CH_2 proton) and 3.79 ppm arise from THF. A very small amount of dimethylamine (2.72 ppm) was observed.

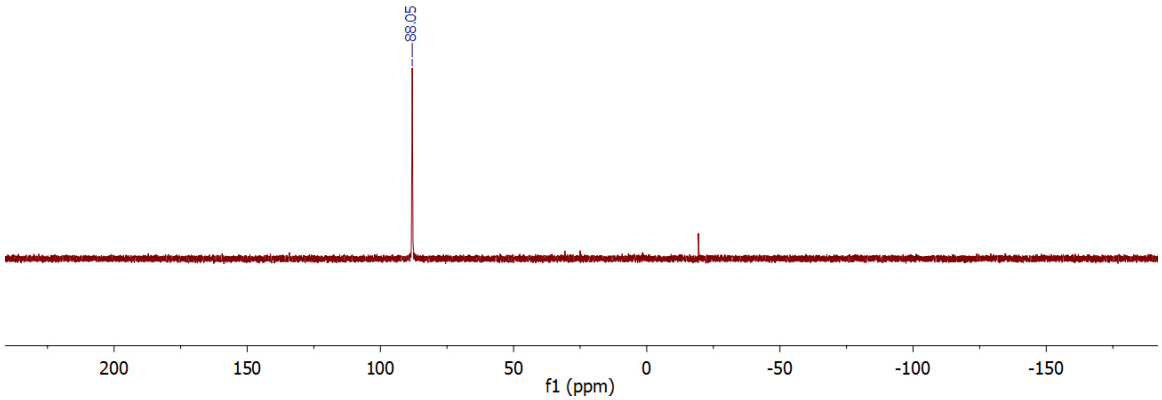

Figure S17. $^{31}P\{^1H\}$ NMR (161.98 MHz, $CDCl_3$, 298 K) spectrum of $[\{(2\text{-BuO})P(2\text{-py})_2\}LiCl]_2$ ([**5**·LiCl]$_2$).

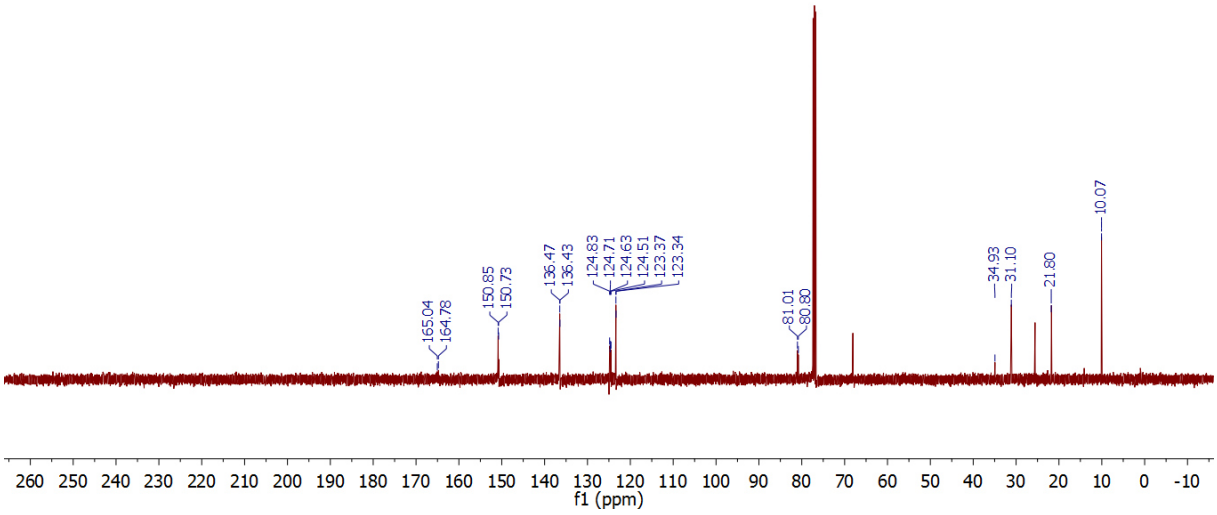

Figure S18. $^{13}C\{^1H\}$ NMR (100.61 MHz, $CDCl_3$, 298 K) spectrum of $[\{(2\text{-BuO})P(2\text{-py})_2\}LiCl]_2$ ([**5**·LiCl]$_2$).

Note: Signals at 68.1 ppm and 25.6 ppm arise from THF.

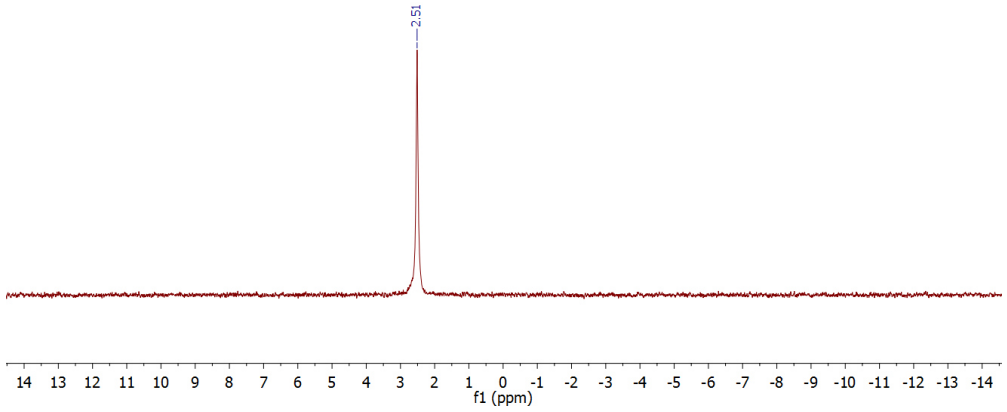

Figure S19. $^{7}Li\{^1H\}$ NMR (155.51 MHz, $CDCl_3$, 298 K) spectrum of $[\{(2\text{-BuO})P(2\text{-py})_2\}LiCl]_2$ ([**5**·LiCl]$_2$).

NMR spectra of (*S*)-(2-BuO)P(2-py)$_2$ (5-*S*)

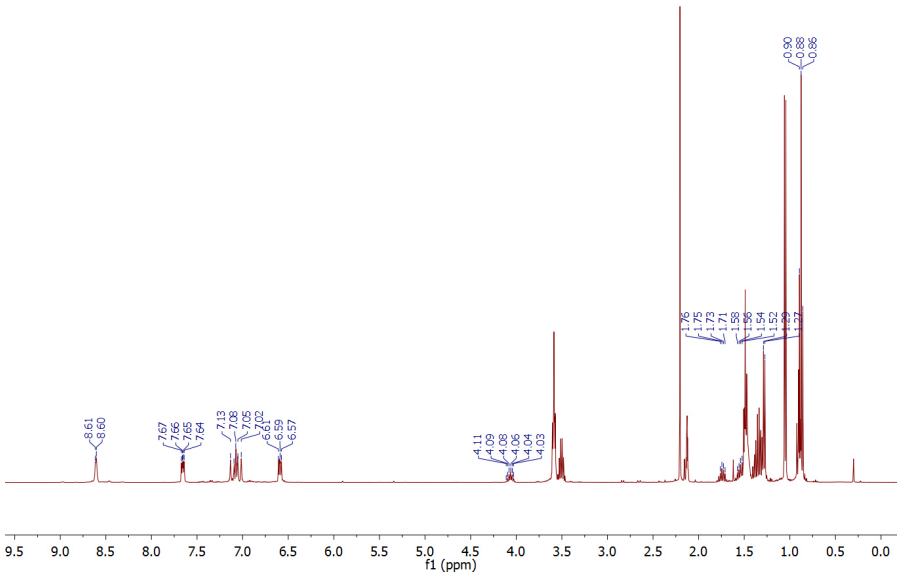

Figure S20. *In situ* ^{1}H NMR (400.13 MHz, d$_8$-tol, 298 K) spectrum of (*S*)-(2-BuO)P(2-py)$_2$ (**5-*S***).

Note: Since the reaction was carried out in a Young's NMR tube, dimethylamine (2.21 ppm), the additional alcohol (3.51 ppm, 1.05 ppm, 1.34 ppm, 0.89 ppm) as well as THF (3.59 ppm and 1.47 ppm) are present in the mixture. Furthermore, the d$_8$-tol signal (7.17 ppm - 6.98 ppm) partially overlaps with the H4 py-signal.

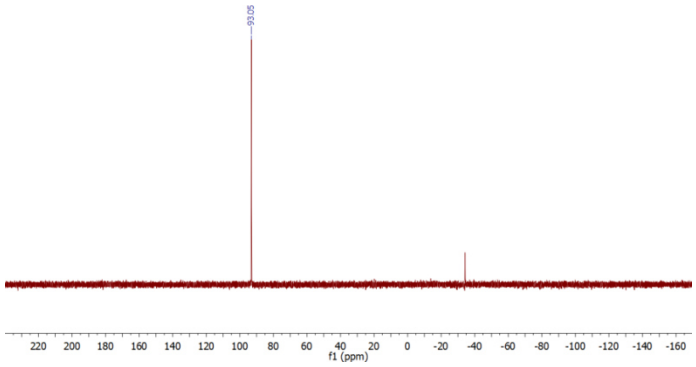

Figure S21. *In situ* ^{31}P{^{1}H} NMR (161.98 MHz, d$_8$-tol, 298 K) spectrum of (*S*)-(2-BuO)P(2-py)$_2$ (**5-*S***).

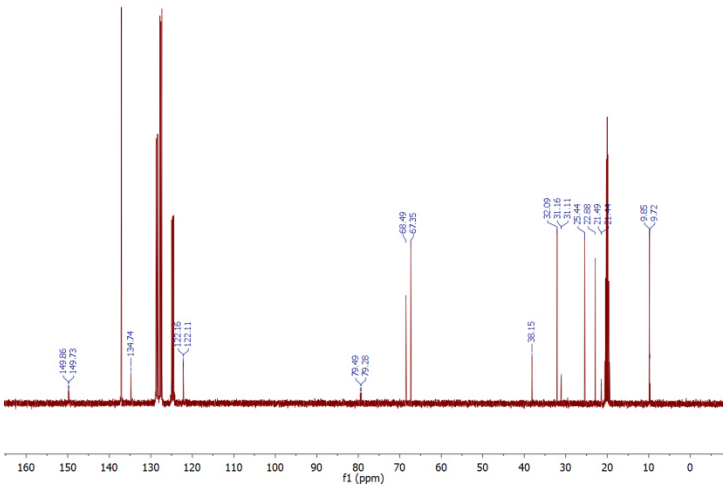

Figure S22. *In situ* ^{13}C{^{1}H} NMR (100.63 MHz, d$_8$-tol, 298 K) spectrum of (*S*)-(2-BuO)P(2-py)$_2$ (**5-*S***).

Note: Since the reaction was carried out in a Young's NMR tube, dimethylamine as well as the additional alcohol are present in the mixture.

NMR spectra of (*R*)-(2-BuO)P(2-py)$_2$ (5-*R*)

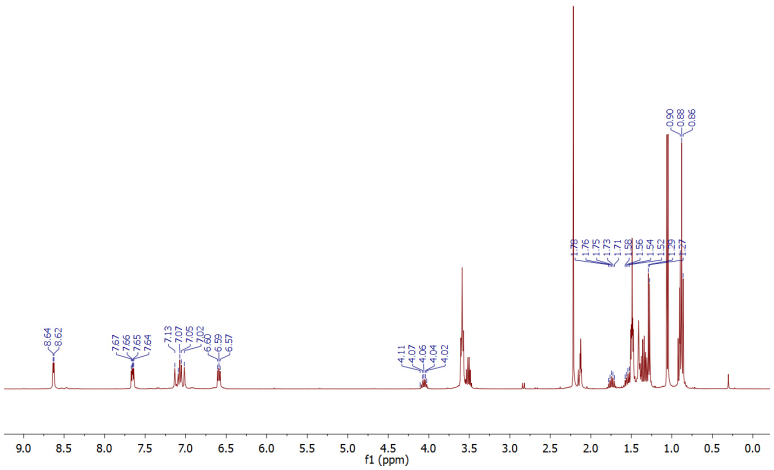

Figure S23. *In situ* ^{1}H NMR (400.13 MHz, d_8-tol, 298 K) spectrum of (*R*)-(2-BuO)P(2-py)$_2$ (**5-*R***).

Note: Since the reaction was carried out in a Young's NMR tube, dimethylamine (2.22 ppm), the additional alcohol (3.51 ppm, 1.06 ppm, 1.35 ppm, 0.89 ppm) as well as THF (3.59 ppm and 1.49 ppm) are present in the mixture. Furthermore, the d_8-tol signal (7.15 ppm - 6.99 ppm) partially overlaps with the H4 py-signal.

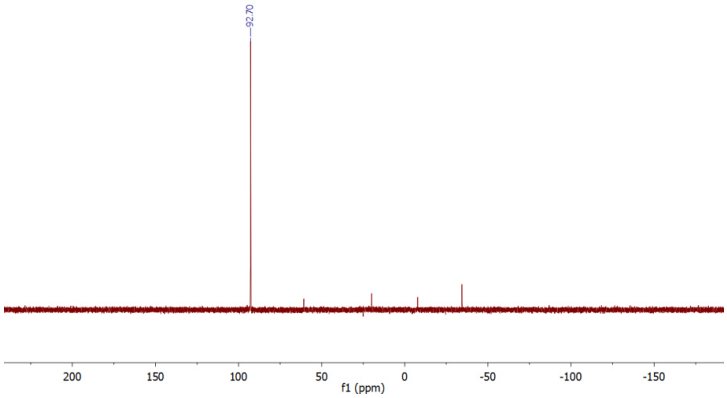

Figure S24. *In situ* ^{31}P{^{1}H} NMR (161.98 MHz, d_8-tol, 298 K) spectrum of (*R*)-(2-BuO)P(2-py)$_2$ (**5-*R***).

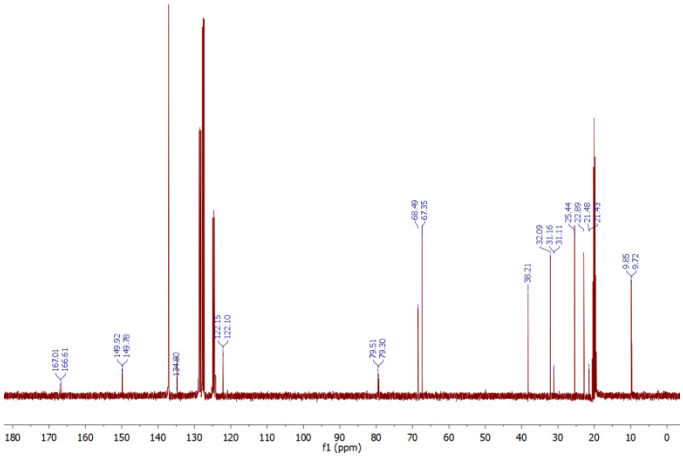

Figure S25. *In situ* ^{13}C{^{1}H} NMR (100.63 MHz, d_8-tol, 298 K) spectrum of (*R*)-(2-BuO)P(2-py)$_2$ (**5-*R***).

Note: Since the reaction was carried out in a Young's NMR tube, dimethylamine as well as the additional alcohol are present in the mixture.

NMR spectra of $(MeO)_2P(2\text{-py})$ (7)

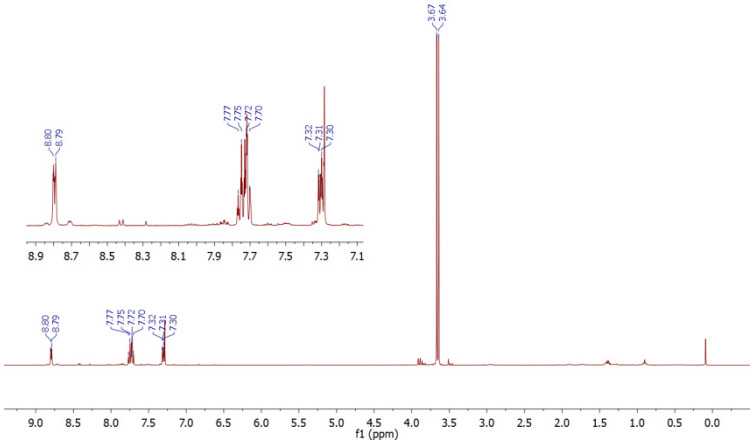

Figure S26. ^{1}H NMR (400.13 MHz, $CDCl_3$, 298 K) spectrum of $(MeO)_2P(2\text{-py})$ (**7**).

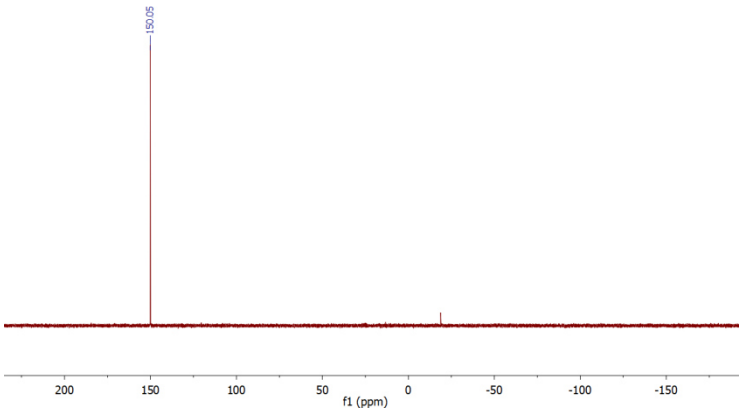

Figure S27. $^{31}P\{^{1}H\}$ NMR (161.98 MHz, $CDCl_3$, 298 K) spectrum of $(MeO)_2P(2\text{-py})$ (**7**).

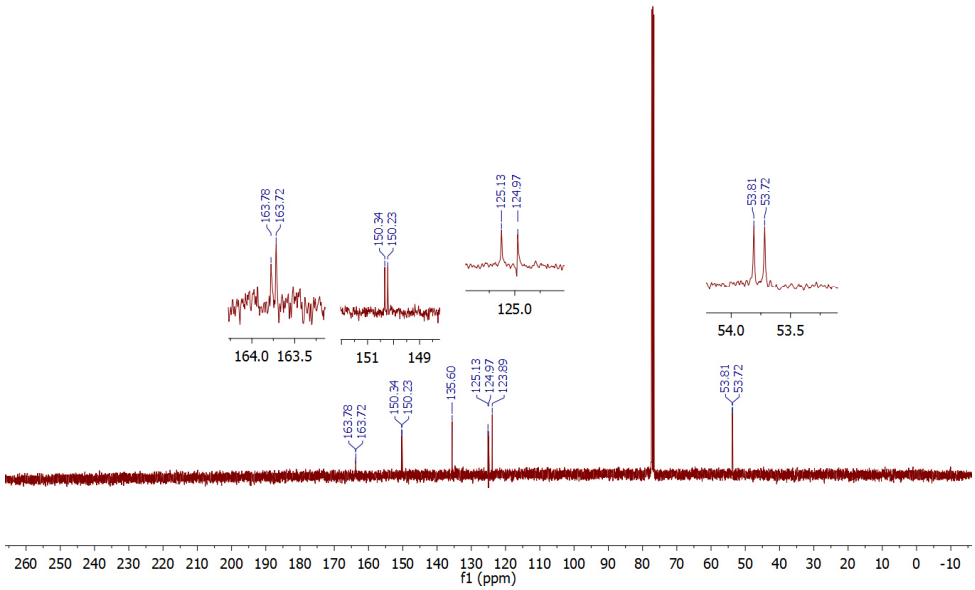

Figure S28. $^{13}C\{^{1}H\}$ NMR (100.62 MHz, $CDCl_3$, 298 K) spectrum of $(MeO)_2P(2\text{-py})$ (**7**).

NMR spectra of $(Et_2N)(PhO)P(2\text{-py})$ (8)

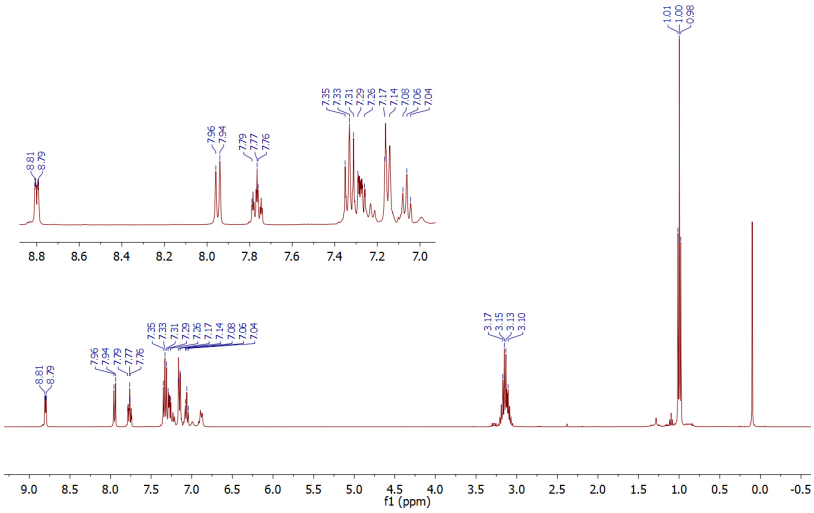

Figure S29. ^{1}H NMR (400.13 MHz, $CDCl_3$, 298 K) spectrum of $(Et_2N)(PhO)P(2\text{-py})$ (**8**).

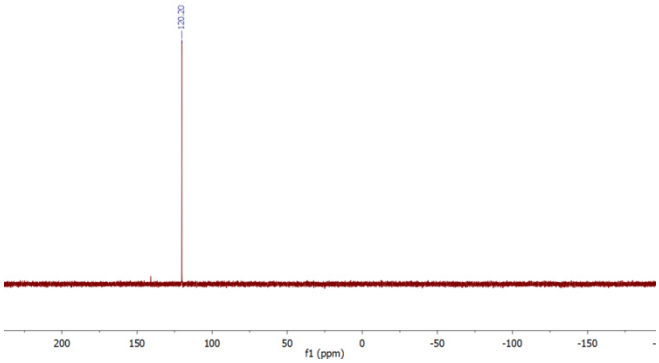

Figure S30. $^{31}P\{^{1}H\}$ NMR (161.98 MHz, $CDCl_3$, 298 K) spectrum of $(Et_2N)(PhO)P(2\text{-py})$ (**8**).

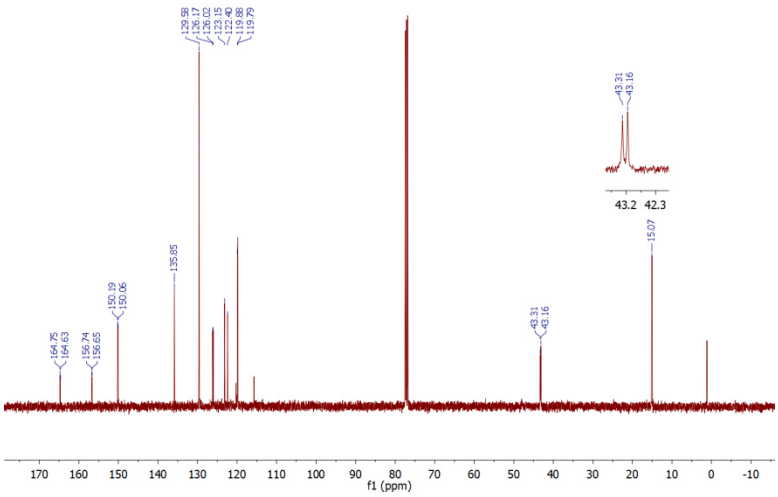

Figure S31. $^{31}C\{^{1}H\}$ NMR (100.61 MHz, $CDCl_3$, 298 K) spectrum of $(Et_2N)(PhO)P(2\text{-py})$ (**8**).

NMR spectra of $(PhO)_2P(2\text{-py})$ (9)

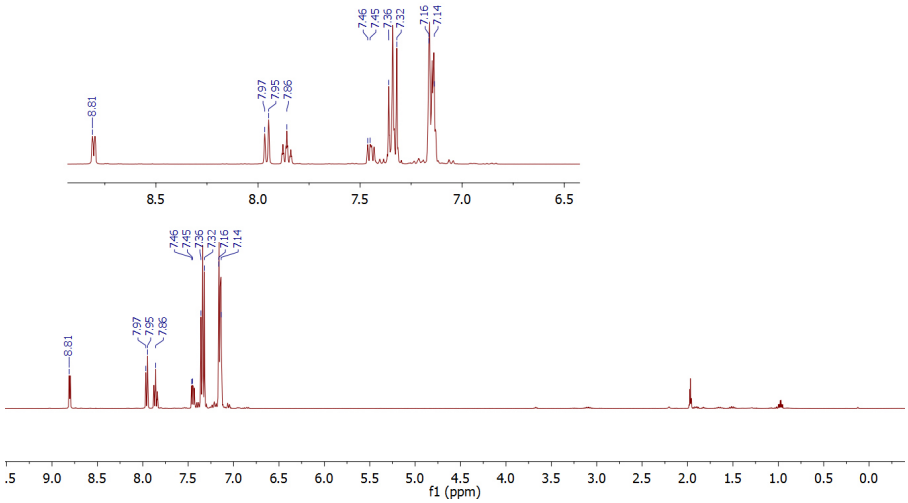

Figure S32. ^{1}H NMR (400.13 MHz, CD_3CN, 298 K) spectrum of $(PhO)_2P(2\text{-py})$ (**9**).

Note: The multiplet at 0.98 ppm results from residual diethylamine.

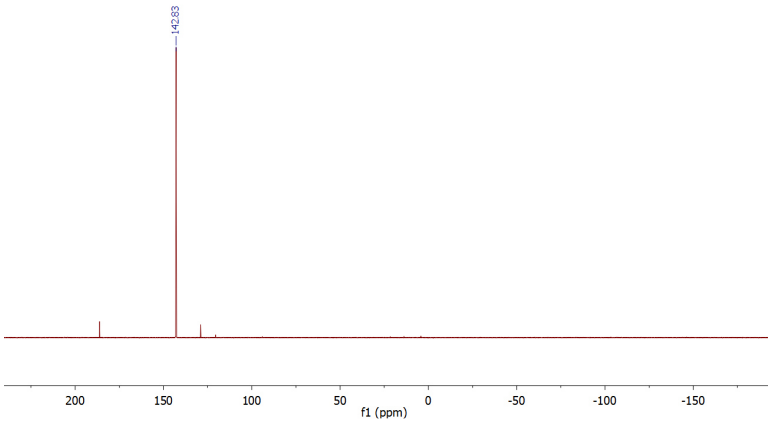

Figure S33. $^{31}P\{^{1}H\}$ NMR (161.98 MHz, CD_3CN, 298 K) spectrum of $(PhO)_2P(2\text{-py})$ (**9**).

Note: A small amount of impurities (4 %) was observed, since **9** is readily oxidised/hydrolysed.

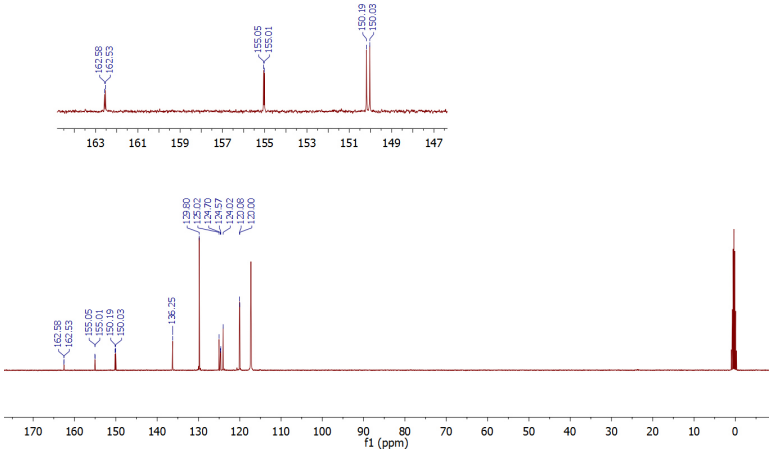

Figure S34. $^{13}C\{^{1}H\}$ NMR (100.63 MHz, CD_3CN, 298 K) spectrum of $(PhO)_2P(2\text{-py})$ (**9**).

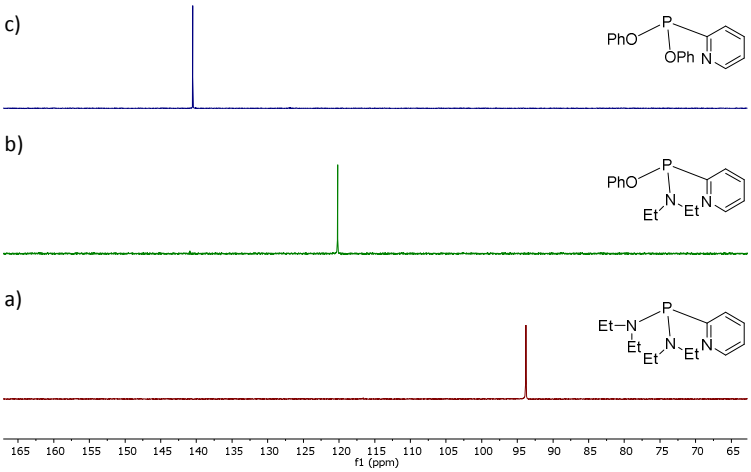

Figure S35. $^{31}P\{^{1}H\}$ NMR spectra showing the reaction progress of **2** with PhOH; (a) the pure starting material, (b) addition of 1 eq of PhOH at reflux in toluene, (c) addition of a further equivalent of PhOH.

b) NMR spectra of the copper(I) phosphine complexes

NMR spectra of [(MeCN)Cu{(Et$_2$N)$_2$P(2-py)}]$_2$(PF$_6$)$_2$ (10)

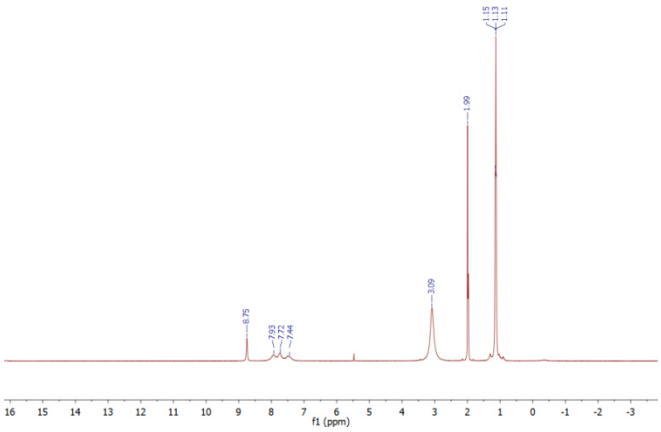

Figure S36. ^{1}H NMR (400.14 MHz, CD$_3$CN, 298 K) spectrum of [(MeCN)Cu{(Et$_2$N)$_2$P(2-py)}]$_2$(PF$_6$)$_2$ (**10**).

Note: The singlet at 5.48 ppm results from CH_2Cl_2.

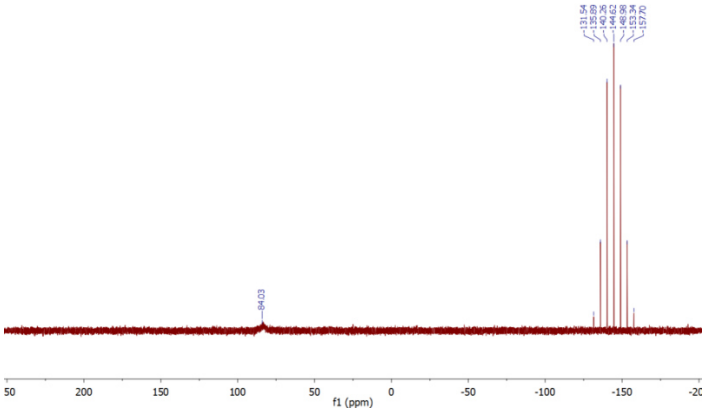

Figure S37. ^{31}P{^{1}H} NMR (161.98 MHz, CD$_3$CN, 298 K) spectrum of [(MeCN)Cu{(Et$_2$N)$_2$P(2-py)}]$_2$(PF$_6$)$_2$ (**10**).

Note: ^{13}C{^{1}H} NMR spectrum could not be obtained due to extensive line broadening.

NMR spectra of [(MeCN)Cu{(Et$_2$N)(PhO)P(2-py)}]$_2$(PF$_6$)$_2$ (12)

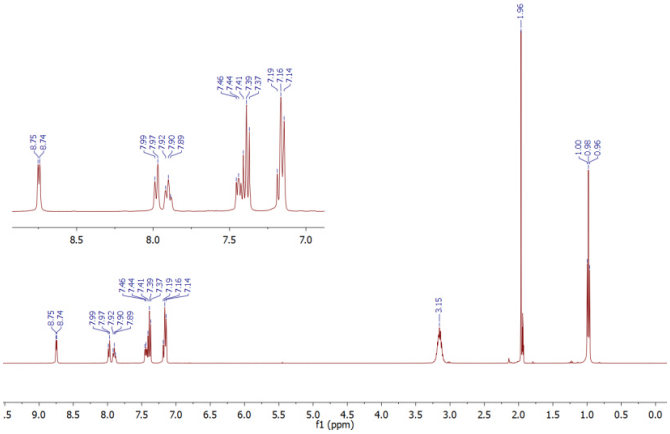

Figure S38. ^{1}H NMR (400.14 MHz, CD$_3$CN, 298 K) spectrum of [(MeCN)Cu{(Et$_2$N)(PhO)P(2-py)}]$_2$(PF$_6$)$_2$ (**12**).

Note: The d_3-acetonitrile solvent residual signal partially overlaps with the signal of the coordinated CH_3CN molecules at 1.96 ppm.

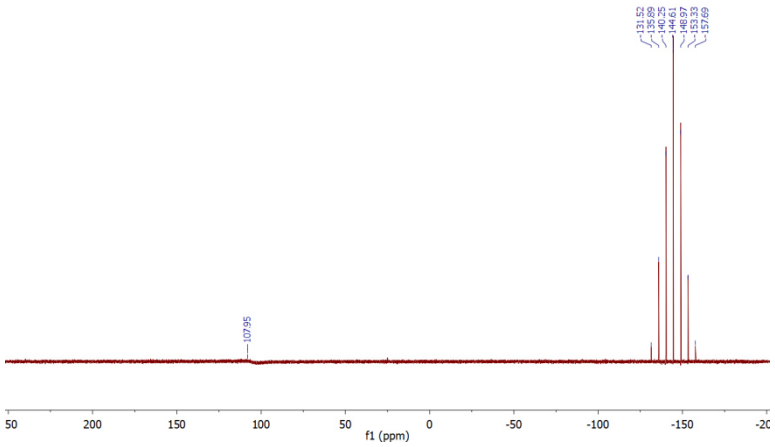

Figure S39. $^{31}P\{^1H\}$ NMR (161.98 MHz, CD_3CN, 298 K) spectrum of $[(MeCN)Cu\{(Et_2N)(PhO)P(2\text{-}py)\}]_2(PF_6)_2$ (**12**).

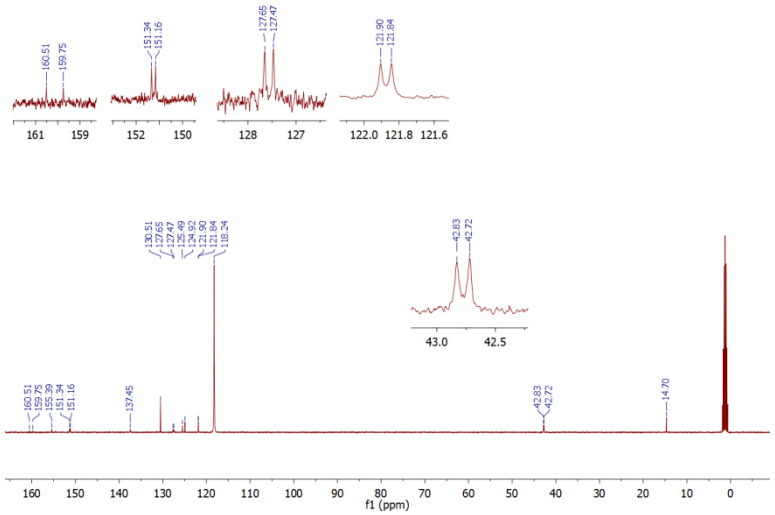

Figure S40. $^{13}C\{^1H\}$ NMR (100.61 MHz, CD_3CN, 298 K) spectrum of $[(MeCN)Cu\{(Et_2N)(PhO)P(2\text{-}py)\}]_2(PF_6)_2$ (**12**).

Note: The solvent residual peak of d_3-acetonitrile (septet at 1.3 ppm) overlaps with the signal of the coordinated CH_3CN molecules (0.76 ppm), which was confirmed by a ^{13}C DEPT experiment. The same observation was made for the second solvent residual peak of acetonitrile, which also overlaps with the signal of the coordinated CH_3CN molecules at 118.2 ppm.

NMR spectra of [(MeCN)Cu$_2${(PhO)$_2$P(2-py)}$_3$](PF$_6$)$_2$·3THF (13·3THF)

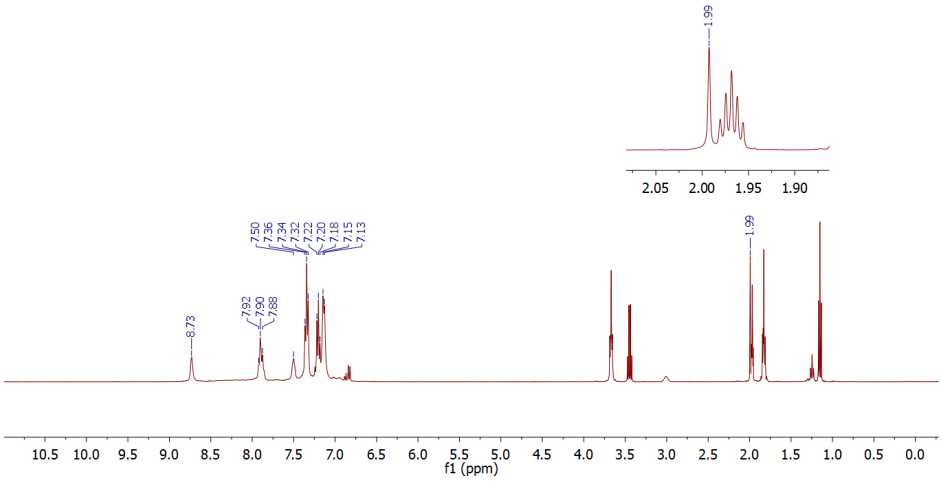

Figure S41. ^{1}H NMR (400.13 MHz, CD$_3$CN, 298 K) spectrum of [(MeCN)Cu$_2${(PhO)$_2$P(2-py)}$_3$](PF$_6$)$_2$·3THF (**13**·3THF).

Note: The d$_3$-acetonitrile solvent residual signal partially overlaps with the signal of the coordinated CH$_3$CN molecules. Furthermore, signals of THF (1.83 ppm, 3.67 ppm) and diethyl ether (1.15 ppm, 3.45 ppm) are present in the sample from crystallisation. Also a very small amount of free PhOH (6.81 ppm - 6.90 ppm) was observed.

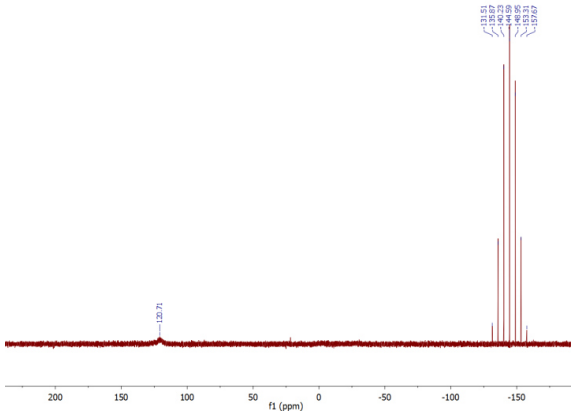

Figure S42. ^{31}P{^{1}H} NMR (161.98 MHz, CD$_3$CN, 298 K) spectrum of [(MeCN)Cu$_2${(PhO)$_2$P(2-py)}$_3$](PF$_6$)$_2$·3THF (**13**·3THF).

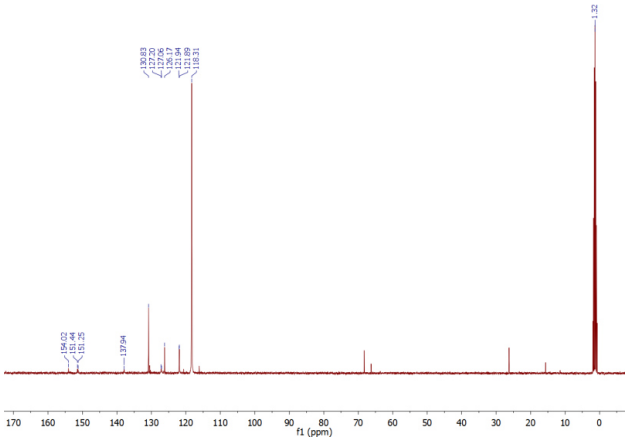

Figure S43. ^{13}C{^{1}H} NMR (100.63 MHz, CD$_3$CN, 298 K) spectrum of [(MeCN)Cu$_2${(PhO)$_2$P(2-py)}$_3$](PF$_6$)$_2$·3THF (**13**·3THF).

Note: The $^{13}C\{^1H\}$ NMR of the quaternary carbon atom of the pyridyl ring could not be observed due to line-broadening. Again, as seen in the ^1H NMR spectrum of **13**·3THF diethyl ether (15.87 ppm, 66.34 ppm) and THF (26.33 ppm, 68.33 ppm) are present in the spectrum.

NMR spectra of [{OP(O)(H)(2-py)}Cu_2{(PhO)$_2$P(2-py)}$_2$](PF$_6$)$_2$·2THF (14·2THF)

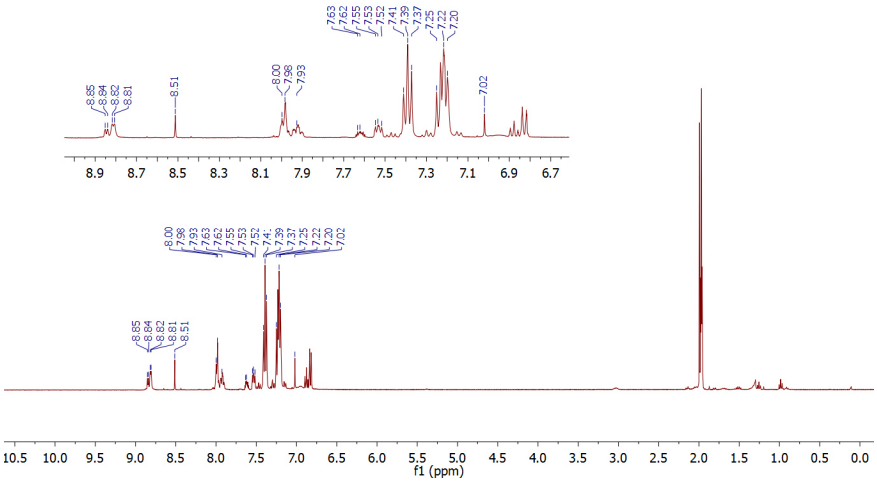

Figure S44. ^1H NMR (400.13 MHz, CD_3CN, 298 K) spectrum of [{OP(O)(H)(2-py)}Cu_2{(PhO)$_2$P(2-py)}$_2$]$_2$(PF$_6$)$_2$ (**14**·2THF).

Note: At 1.99 ppm the d_3-acetonitrile solvent residual signal partially overlaps with the signal of CH_3CN (was used as solvent during the reaction). Also free PhOH (6.81 - 6.90 ppm) (from the hydrolysis of L2) was observed.

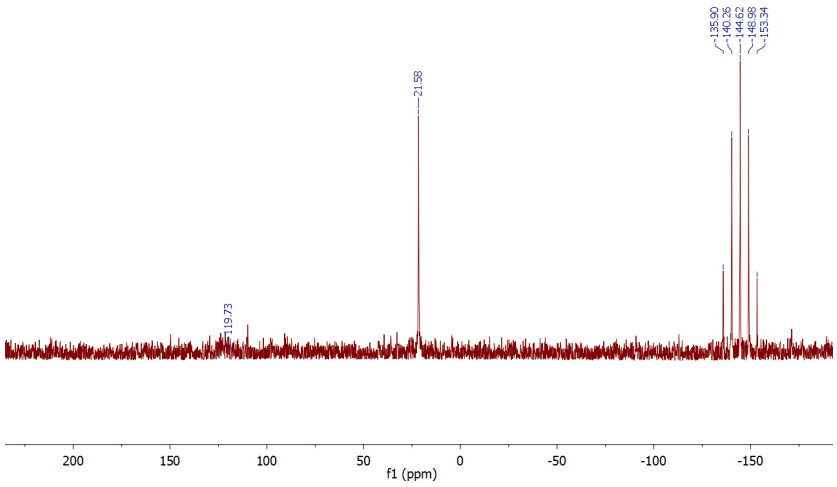

Figure S45. $^{31}P\{^1H\}$ NMR (161.98 MHz, CD_3CN, 298 K) spectrum [{OP(O)(H)(2-py)}Cu_2{(PhO)$_2$P(2-py)}$_2$]$_2$(PF$_6$)$_2$ (**14**·2THF).

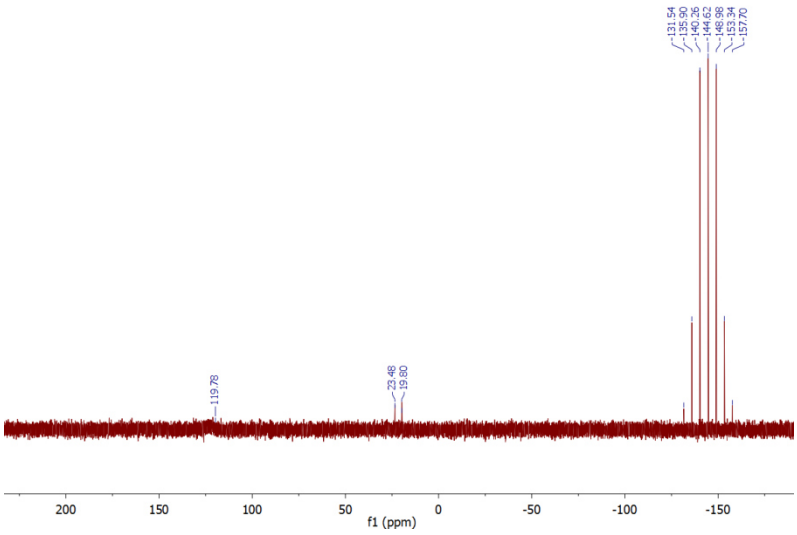

Figure S46. ^{31}P NMR (161.98 MHz, CD_3CN, 298 K) spectrum of $[\{OP(O)(H)(2\text{-py})\}Cu_2\{(PhO)_2P(2\text{-py})\}_2]_2(PF_6)_2$ (**14**·2THF).

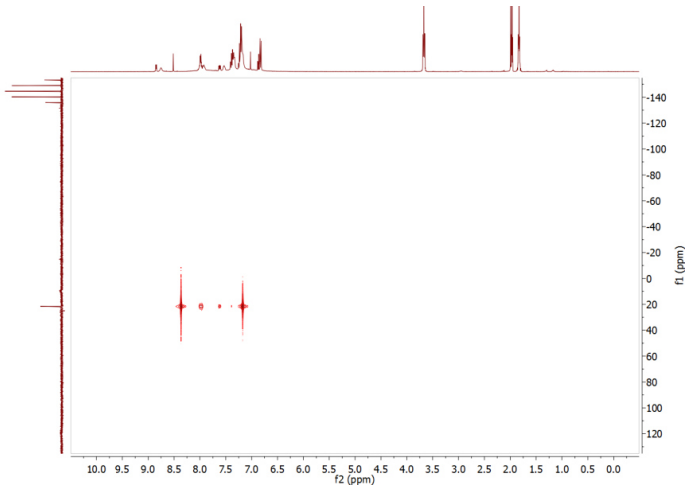

Figure S47. ^{31}P-^{1}H HMBC NMR (500.20 MHz, CD_3CN, 298 K) spectrum of $[\{OP(O)(H)(2\text{-py})\}Cu_2\{(PhO)_2P(2\text{-py})\}_2]_2(PF_6)_2$ (**14**·2THF).

4. Single-crystal X-ray crystallography

CCDC Numbers

1	4	5	10	11	12	13	14
1505957	1505955	1505960	1505962	1505959	1505956	1505961	1505958

Crystal-Structure Refinement

All single-crystal X-ray data were measured at 180(2) K on a Bruker D8-Quest diffractometer equipped with a I□S Cu microsource and a Photon-100 detector. Data collection and processing were carried out using the APEX2/APEX3 packages. Structure solution and refinement were carried out using SHELXT and SHELXL.

Refinement was straightforward for **1**, **4**, **10**, **11** and **12**.

For **5**: the 2-butoxide group were modelled in two orientations, with the terminal C atoms in the two orientations (C2/C4) constrained to lie at the same position. To control the geometry, the bond distances and 1,3-distances were restrained to standard values. All of the (non-H) atoms were refined anisotropically, but with the application of ISOR restraints.

For **13**: one PF_6^- anion was modelled as disordered over two orientations with a common P atom position. The other PF_6^- anion did not seem to exhibit the same degree of rotational disorder, and was modelled with a single orientation. All P–F distances in both anions were restrained to a common refined value. A reasonable octahedral geometry was maintained without restraints on the F...F distances. All F atoms were refined anisotropically, with the application of ISOR restraints.

Three solvent THF molecules are present, one of which is disordered about an inversion centre. All of the bond distances were restrained to standard values, and all of the non-H atoms were refined anisotropically, with ISOR restraints. For one THF site, a superimposed diethylether molecule was clearly visible and included with all bond distances and 1,3-distances restrained to standard values. All atoms were refined anisotropically, with ISOR restraints.

For **14**: the one PF_6^- anion was modelled as disordered over two orientations with a common P atom position. All P–F distances were restrained to a common refined value, but restraints on F...F distances were not applied. All F atoms were refined anisotropically, with the application of ISOR restraints.

Two solvent THF molecules are present. All of the bond distances were restrained to standard values, and all of the non-H atoms were refined anisotropically, with ISOR restraints.

Table S1: Crystallographic parameters of the ligands [**1**(LiCl)$_3$·2THF]$_2$, [**4**·LiCl]$_2$ and [**5**·LiCl]$_2$.

Compound reference	[**1**(LiCl)$_3$·2THF]$_2$	[**4**·LiCl]$_2$	[**5**·LiCl]$_2$
Chemical formula	$C_{40}H_{60}Cl_6Li_6N_6O_4P_2$	$C_{22}H_{22}Cl_2Li_2N_4O_2P_2$	$C_{28}H_{34}Cl_2Li_2N_4O_2P_2$
Formula mass	1005.22	521.15	605.31
Crystal system	triclinic	monoclinic	monoclinic
a/Å	10.9913(3)	9.6580(3)	19.1423(14)
b/Å	11.7487(3)	13.2919(4)	8.0771(6)
c/Å	12.2632(4)	10.1121(3)	22.2684(18)
α/°	105.4860(14)	90	90
β/°	99.1063(14)	98.7640(10)	104.894(4)
γ/°	115.1390(13)	90	90
Unit cell volume/Å^3	1312.84(7)	1282.97(7)	3327.3(4)
Temperature/K	180(2)	180(2)	180(2)
Space group	*P*–1	*P*2$_1$/*n*	*I*2/*a*
Z	1	2	4
Radiation type	CuKα	CuKα	CuKα
Absorption coefficient, μ/mm^{-1}	3.894	3.670	2.896
No. of reflections measured	36815	17882	33730
No. of independent reflections	4628	2262	2405
R_{int}	0.053	0.036	0.101
Final R1 values (I > 2σ(I))	0.046	0.037	0.072
Final wR(F^2) values (I > 2σ(I))	0.115	0.103	0.177
Final R1 values (all data)	0.063	0.042	0.109
Final wR(F^2) values (all data)	0.125	0.106	0.204
Goodness of fit on F^2	1.05	1.07	1.06

Table S2: Crystallographic parameters of the Cu^{I} complexes **11**·MeOH, **12**, **13**·3THF and **14**·2THF

Compound reference	**10**	**11**·MeOH	**12**	**13**·3THF	**14**·2THF
Chemical formula	$C_{30}H_{54}Cu_2F_{12}N_8P_4$	$C_{24}H_{30}Cl_2Cu_2N_4O_4P_2$	$C_{34}H_{44}Cu_2F_{12}N_6O_2P_4$	$C_{63}H_{65.64}Cu_2F_{12}N_4O_{8.5}P_5$	$C_{94}H_{96}Cu_4F_{12}N_6O_{16}P_8$
Formula mass	1005.77	698.44	1047.71	1524.77	2295.68
Crystal system	monoclinic	triclinic	monoclinic	triclinic	monoclinic
a/Å	11.0995(5)	8.9283(5)	10.3510(2)	14.9241(5)	13.4157(4)
b/Å	9.0222(5)	9.4929(6)	10.4256(2)	15.6614(5)	18.3267(6)
c/Å	21.4868(10)	9.5208(6)	20.5378(4)	15.8894(5)	20.2257(6)
α/°	90	108.092(3)	90	96.5105(17)	90
β/°	94.122(2)	109.909(2)	92.8680(10)	105.7917(16)	91.5450(18)
γ/°	90	91.050(3)	90	99.4915(16)	90
Unit cell volume/Å^3	2146.16(18)	714.22(8)	2213.57(7)	3475.4(2)	4971.0(3)
Temperature/K	180(2)	180(2)	180(2)	180(2)	180(2)
Space group	*P*2$_1$/*c*	*P*–1	*P*2$_1$/*c*	*P*–1	*P*2$_1$/*n*
Z	2	1	2	2	2
Radiation type	CuKα	CuKα	CuKα	CuKα	CuKα
Absorption coefficient, μ/mm^{-1}	3.406	4.938	3.358	2.607	2.950
No. of reflections measured	36582	18128	24637	90535	52568
No. of independent reflections	3796	2529	3921	12274	8723
R_{int}	0.040	0.046	0.036	0.045	0.067
Final R1 values (I > 2σ(I))	0.043	0.032	0.029	0.049	0.074
Final wR(F^2) values (I > 2σ(I))	0.111	0.085	0.071	0.128	0.159
Final R1 values (all data)	0.050	0.037	0.036	0.067	0.105
Final wR(F^2) values (all data)	0.115	0.089	0.076	0.141	0.179
Goodness of fit on F^2	1.04	1.09	1.02	1.02	1.06